Detection and discrimination of nanoparticles using bullet shape nanopores coated with PEG

Saly Charles-Achille, Nathan Meyer, Imad Abrao-Nemeir, Mathilde Lepoitevin, Joan Torrent, Jean-Marc Janot, Sébastien Balme

Discrimination of nanoparticles using bullet shape nanopores coated with PEG

Saly Charles-Achille[1], Nathan Meyer[1,2], Imad Abrao-Nemeir[1], Mathilde Lepoitevin[3], Joan Torrent[2], Jean Marc Janot[1], Sébastien Balme*[1]

[1] *Institut Européen des Membranes, UMR5635 University of Montpellier ENCSM CNRS, Place Eugène Bataillon, 34095 Montpellier cedex 5, France.*

[2] *INM, University of Montpellier , INSERM, Montpellier, France*

[3] *Institut des Matériaux Poreux de Paris (IMAP), UMR 8004 CNRS, Ecole Normale Supérieure de Paris, Ecole Supérieure de Physique et de Chimie Industrielles de Paris, PSL Université, 75005 Paris, France*

Abstract

The use of single track-etched nanopores to distinguish molecules is limited by the difficulty in comparing independent experiments. This is mainly because the properties (size, surface state) among various equivalent nanopores are not strictly identical. In this work, we propose a way to discriminate different sized gold nanoparticles coated with PEG from 38 to 90 nm. using bullet-like shape nanopores with with tip diameters of 100 and 130 ± 30 nm, functionalized with polyethylene glycol (PEG) chains of different lengths (5 and 20 kDa),.. We show that the two classical parameters of current pertubation (the relative blockade amplitude and the dwell time) caused by the interaction of the nanoparticles with the nanopore allow the discrimination of the nanoparticles using each nanopore independently. Indeed, both the nanopore diameter and the PEG length influence the current blockade parameter. To concatenate data from the different independent experiments, the current blockade were characterized by 8 features including the amplitude relative, the dwell time, the area, the slope of the blockade and 3 features related to the experimental conditions (applied voltage, the nanopore diameter and the PEG molecular weight). The dataset was built by summing all the events of the different experiments. Using a supervised neuronal network classification, we achieved 99.4% accuracy in learning and 100% in testing, showing that it is possible to distinguish nanoparticles from independent experiments despite the inherent variability of the track-etched nanopores.

Keywords: Nanopore, track-etched, supervised classification, single molecule sensing

Introduction

For the last twenty years, artificial nanopores (solid-state or polymer) have provided an alternative to label-free single-molecule detection [1–4]. A classical single molecule detection experiment consists of applying a constant voltage across a single nanopore and recording the current generated by the transport of electrolytes [5,6]. As an object crosses through the pore, it induces an ionic current perturbation whose amplitude and time parameters depend on its intrinsic properties *i.e.* volume, shape, and charge [7,8], but also on its position in the pore [9,10]. This technique called resistive pulse sensing allows the detection of a large number of analytes in solution at the single molecule level, as long as the size and charge of the pore and the object are compatible [7,11–13]. Thus, by judiciously choosing the diameter, aspect ratio, and surface state of the artificial nanopore, they become a powerful tool to analyse objects such as amyloids [14,15], nanoparticles [13,16–21], and viruses [22,23].

Among artificial nanopores, those obtained from polymers by the track-etching technique are particularly interesting since their geometries can easily be adapted by modifying the chemical etching conditions [24,25]. To go into the details of the design of the single polymer nanopores, the technique consists of a first step where the film is irradiated by heavy ion irradiation. The energy dissipated by this ion creates defects in the material which are then revealed by an etching solution [24]. A chemical etching under symmetrical conditions makes it possible to obtain cylindrical nanopores that are perfectly adapted for fundamental studies of ionic transport [26,27]. More interestingly, an asymmetric opening of the nanopores allows the fabrication of conical or even "bullet-like" geometries that exhibit ionic diode properties [28,29]. To summarize, an ionic diode exhibit a non-linear current/voltage response induced by a heterogeneous distribution of electrolytes in the nanopore [30,31]. This response is extremely sensitive to the surface charge of the nanopore [32]. In the case of PET, the most widely used polymer to obtain ionic diodes, after chemical etching the surface is covered with carboxylate groups which induce a negative surface charge estimated to 0.01 C/m^2 from analytical models applied to cylindrical nanopores [26]. On the other hand, these carboxylate functions serve as a reactive function for the chemical modification of the nanopore, thus offering a wide range of simple chemical reactions in the aqueous phase, such as condensation with an amine, which has been the most reported in the literature [33]. Thus, they have been widely exploited for sensor design due to the simplicity to functionalize their surface and the sensitivity of the ionic diode to surface modification [33,34]. Compared to solid-state nanopores and nanopipettes, the track-etched nanopores are not widely used for resistive pulse sensing because of their low resolution to detect small objects such as proteins or DNA. Nevertheless, they have shown their efficiency in the detection of amyloids [35–37] or nanoparticles [38,39]. The main limitation of track-etched nanopores for molecule identification comes from the difficulty to reproduce experiments under strictly the same conditions. Indeed, it is difficult to know the exact size of the nanopore for any etching condition because there is some variability in the diameter and the angle. Moreover, for the asymmetrically shaped nanopore i.e. conical or bullet-like, the non-linear current-voltage dependence makes it difficult to define the exact diameter. Particularly, in the

conical nanopore, it is impossible to know *a priori* the diameter. This is not the case for the bullet shape geometry because the chemical etching is performed under symmetrical condition and thus can be calibrated. Nevertheless, a certain variability has to be taken into account. On the contrary, biological nanopores, are always identical, which easily allows the summation of events from several independent experiments of the same analyte. For the track-etched nanopores, a large number of nanopores have to be open to obtain a significant number of similar ones, limiting their application. In this work, we aim to assess the use of machine learning to circumvent the difficulty of nanopore reproducibility. In other words, is it possible to discriminate nanoparticles using different nanopore sizes by applying different voltages from a unique dataset?

The use of artificial intelligence to improve the resolution of solid-state nanopores involves two approaches. The simplest consists to perform the data processing independently of the classification using machine learning [40,41]. The second one involves deep learning where the data analysis is based on a recognition of current blocking patterns and a classification phase [22,23,42]. This requires a complete rethinking of the signal processing approach. In this approach, the signal that comes from various nanopores should be comparable to nanopores of similar chemistry and size. While the object in translocation creating the signal should not interact with the nanopore surface. This necessitates to introduce the dwell time in the pattern of the current blockade. Thus, it is not suitable for our purpose because we aim to demonstrate the possibility of using different nanopores to detect the same sample. As such, we used machine learning for the classification after the classical detection of events. Therefore, in the data analysis phase, this allows us to get rid of the pattern problem since the experimenter does the signal processing. However, to increase the accuracy of the classification, it becomes necessary to characterize the current blockade by several parameters other than the classical $\Delta I/I_0$ and ΔT [40,41].

In the present work, we aim to discriminate sub-100 nm nanoparticles by combining datasets from independent experiments with different nanopores that present different diameters and polyethylene glycol (PEG) functionalization. To this end, we selected a polymer nanopore with a bullet-like shape geometry that allows obtaining more reproducible nanopores, while having a better signal-to-noise ratio for the detection of nanoparticles. PEG functionalization was used to increase the lifetime of the nanopore, and to reduce its surface charge thus limiting the current rectification. We also used gold nanoparticles coated with PEG to prevent their aggregation under salt solution and applied voltage. The first section is dedicated to the characterization of the nanopores and the nanoparticles. Then, the result of the detection of the nanoparticle using a nanopore with different diameters and PEG chains will be shown and discussed. Finally, the discrimination of the nanoparticles will be discussed using machine learning approaches.

Material and methods

1. Nanopore design and functionalization

The nanopores were obtained using a track-etched technique using polyethylene terephthalate (PET) film, 13 µm thick with biaxial orientation (Goodfellow ref. ES301130). The first step was made by swift heavy ion irradiation (Kr 7 Mev/nucleon) at GANIL (Grand Accélérateur National d'Ions Lourds, Caen). The single nanopore membranes were obtained by irradiating the membrane with a single heavy ion. Note that we also used a multipore membrane for SEM analysis. The chemical etching was performed as follows; the PET film was activated under UV light (λ = 312 nm) for 26 h on one side (called "base"). Then, the film is placed for a few minutes (5 or 6 minutes for the nanopores used) in a NaOH (Sigma-Aldrich ref. S5881) 6 M solution containing 0.05% Dowfax (EZkem ref. E060064) at 60 °C. The result is a track-etched nanopore that exhibits a bullet-like shape. The single nanopores obtained are then functionalized by grafting polyethylene glycol amine (PEG-NH_2, – Nanocs ref. PG1-AM-5k-1 and PG1-AM-20k). To this end, the nanopore was immersed in 5 ml of a solution containing 95 mg MES hydrate (Sigma-Aldrich ref. M8250-25G) 0.1M, 37.5 mg carbodiimide hydrochloride HCl (Anaspec ref. AS-29855) and 250 µl of 2M KCl (Sigma-Aldrich ref. P3911) and a spatula tip of PEG-NH_2 (Mw 5000 of 20000 Da) for 12 h. The current-voltage (I-V) curve was measured at pH 7 using several NaCl concentrations before and after PEG grafting using a patch-clamp amplifier (EPC 10 duo, HEKA electronics, Germany) with Ag/ AgCl electrodes.

2. Gold nanoparticle (AuNP) functionalization and characterization

The AuNP sample was prepared by mixing 2 mL of AuNP 10, 20, and 30 nm solution (Sigma-Aldrich ref. 741957, ref. 741965 and ref. 741973 respectively) with 10 mg PEG-SH (Mw 2000 or 5000 Da, Nanocs ref. PG1-TH-2k-1 and PG1-TH-5k-1 respectively) solubilized in 500 µl of milli-Q water. The solution was stirred for 1 hour. The AuNPs functionalized with PEG (AuNP-PEG) were characterized by UV-vis absorbance using Jasco. Their hydrodynamic radius was determined by diffusion light scattering using PCCP Nanophox. The autocorrelation curve was fitted with the NNLS model.

3. Nanoparticle detection

The nanopore functionalized with PEG moieties was mounted between two compartments of a Teflon cell filled with buffered 1 M NaCl. The AuNP coated with PEG was added to the tip side to reach a concentration between $4{,}4.10^9$ and $1{,}7.10^{10}$ particles/ml. The resistive pulse experiments were performed using a patch-clamp amplifier (EPC 10 duo, HEKA electronics, Germany) with Ag/ AgCl electrodes. The voltage was applied to the working electrode placed in the base side compartment to drive the negatively charged AuNP by electrophoretic force. The ionic currents were recorded at 10 kHz. The signal is filtered at 10 kHz by a Bessel filter. The resistive pulse detection was recorded for at least 30 minutes. The current traces were further analysed to detect events using lab-made software “Peak Nano Tools” developed in Labview using a Bessel filter of 5 kHz. The statistical analysis was then performed using Matlab (2022b) software. The machine

learning was performed using the “statistic and machine learning” toolbox of Matlab (2022b). The data was split into two parts using a random function. In the first one, 80% of events were dedicated to the training and in the second one, 20% of events were used to test the algorithm.

Results and discussion

1. Nanopore characterization

The nanopores were obtained in two steps, irradiation with heavy ions followed by chemical etching with an alkaline solution. To obtain a bullet-like geometry, only one side of the PET film was activated by UV and 0.05% of Dowfax was added to the etching solution. The resulting geometry is due to the surfactant protection of the side not exposed to UVs (called the "tip") that prevents it from chemical etching. To estimate the diameter and the variability of the single nanopores, multipore membranes were produced under strictly the same conditions. The diameter of the tip and base apertures were determined by SEM and plotted on the distribution histograms (Figure 1). Without the addition of Dowfax, the nanopore diameters are centred at 530 nm and 680 nm for etching times of 5 min and 6 min respectively. The addition of Dowfax and the activation of only one side slow the opening of the pores. After 5 minutes of etching, the tip and base diameter are centred on 100 nm and 330 nm respectively. For an etching time of 6 minutes, the diameters are logically larger: 130 nm and 330 nm for the tip and base respectively. The SEM of the cross-sections allows us to characterize the bullet shape of the nanopore (Figure 1). The latter is composed of a cone-like section of length around 500 nm and a cylinder on the rest of the length of the polymer film. These characterizations are in good agreement with that reported by P. Apel [43].

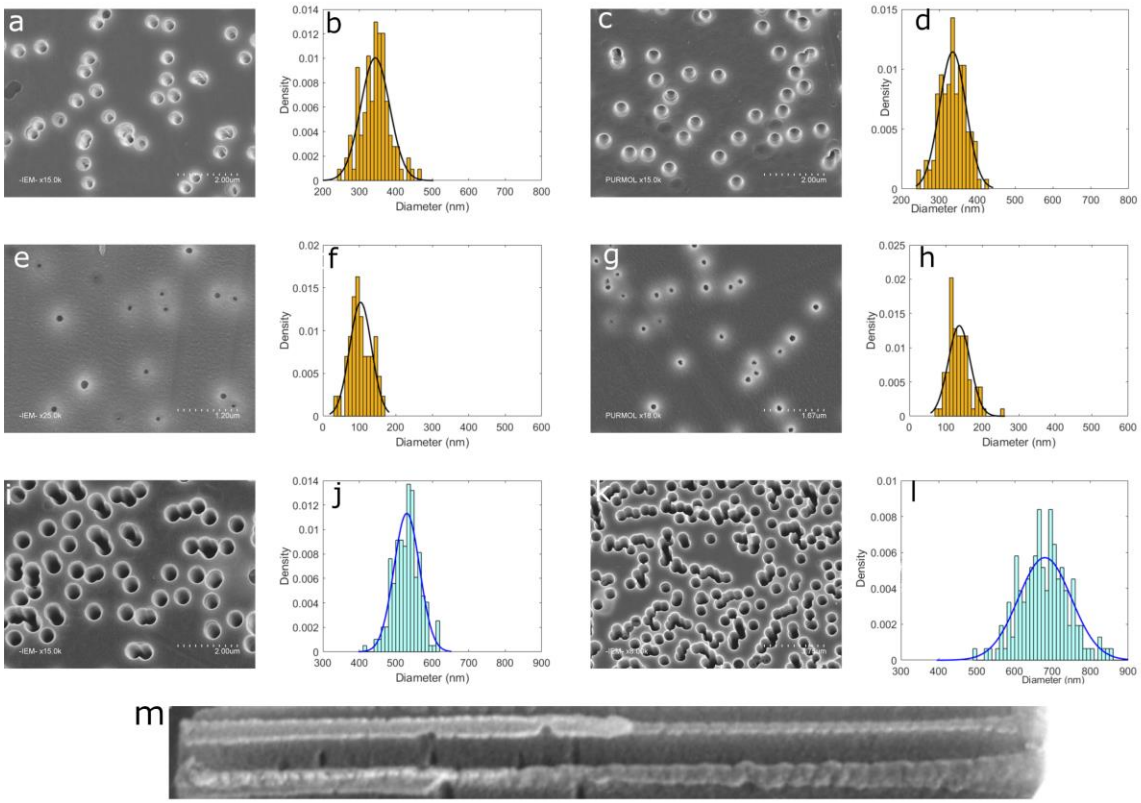

Figure 1: SEM Characterization of bullet-like shape nanopore obtain after 5 min of base (a), tip (e) and the corresponding distribution histogram of nanopore diameter (b) and (f). SEM Characterization of bullet-like shape nanopore obtain after 6 min of base (c), tip (g) and the corresponding distribution histogram of nanopore diameter (d) and (h). SEM Characterization of cylindrical nanopore obtain after chemical etching 5 min (i) and 6 min (k) and the corresponding distribution histogram of nanopore diameter (j) and (l). (m) Cross-section of bullet-like shape nanopore.

After opening, the nanopores were functionalized with PEG chains of different lengths (5 and 20 kDa). To confirm the success of the functionalization, the IV dependence before and after PEG grafting was measured and plotted in Figure 2. After chemical etching, the nanopore exhibits negative surface charges due to the carboxylate moieties inducing the ionic current rectification. The PEG grafting replaced the negative charge with neutral moieties, and thus, the ionic current rectification becomes less pronounced as shown in Figure 2. To evaluate the density of PEG, we measure the conductance at various salt concentrations of cylindrical nanopores with a diameter of about 100 nm before and after functionalization (Figure 2). The conductivity plateau observed at low salt concentration is mainly attributed to the cations present in the nanopore that counterbalance the surface charge (σ). A decrease of the value after PEG grafting occurred meaning that the nanopore is less charged. This confirms the decrease of ionic current rectification observed previously on the bullet shape nanopore. To go further we measure the PEG grafting rate that can be deduced from the surface charge. The latter can be measured exactly from conductance (G) as a function of salt concentration by the hybrid approach expression previously reported [27].

$$G = \kappa_{hyb} \frac{\pi R}{L} \qquad (1)$$

where κ_{hyb} was previously given (see eq. 13 of ref [27]), R the radius, and L the length of the pore.

The fits performed on seven independent cylindrical nanopores show a surface charge of 0.012 ± 0.002 C/m^2 after chemical etching. Assuming that the PEG is uncharged and has replaced the carboxylate moieties, the grafting rate can be deduced directly from the ratio of surface charge measured after and before functionalization. In our experiment 43 % and 27.5 % are found for PEG 5 kDa and 20 kDa respectively, correlate well with the results [26]. The lower value of the functionalization rate for the PEG 20 kDa can be directly correlated with its larger hydrodynamics volume.

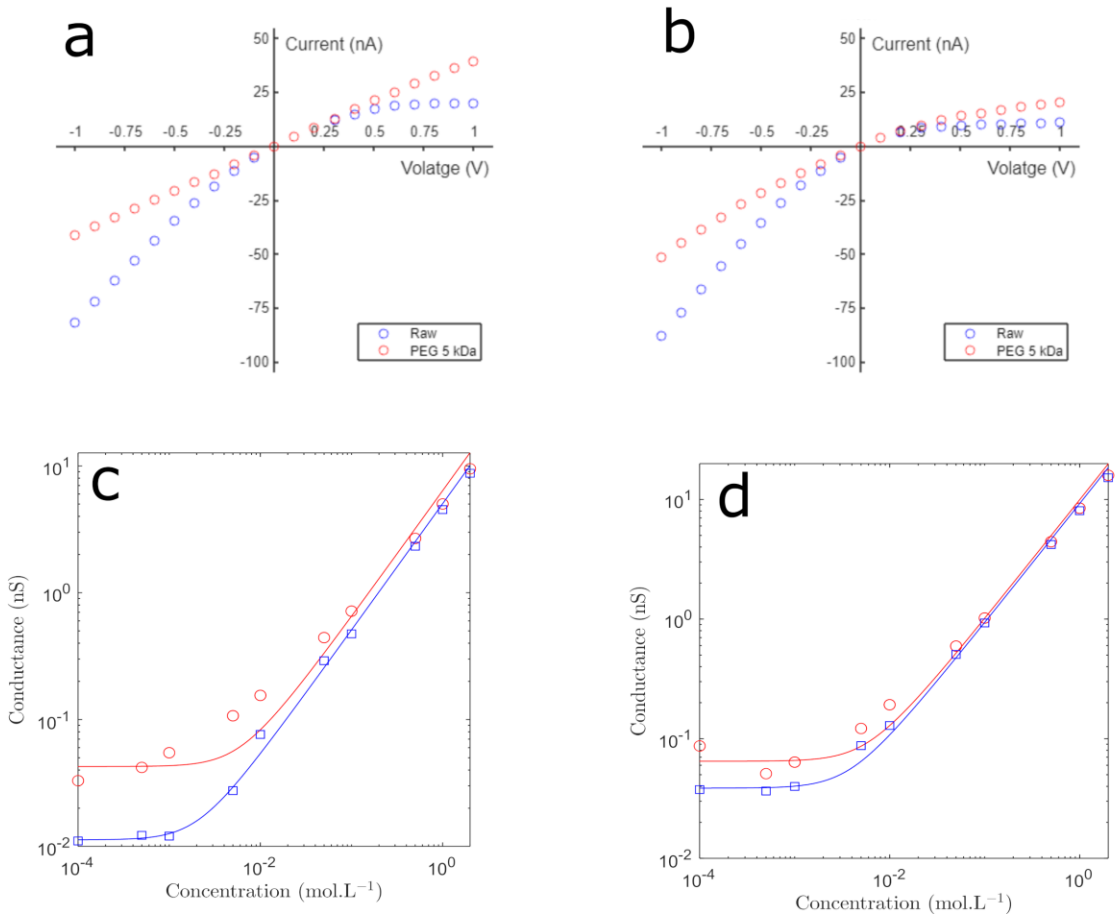

Figure 2: Characterization of nanopore PEG grafting. IV dependence recorded for NaCl 0.1 M before (blue, circle) and after (red, circle) grafting PEG 5 kDa recorded for bullet shape nanopore etched (a) 5 min and (b) 6 min. Conductance as a function of NaCl concentration before (red, circle) and (after, blue square) grafting PEG (c) 5 kDa and (d) 20 kDa recorded for cylindrical nanopore with diameter about 100 nm.

2. AuNP-PEG characterization

AuNPs are known to aggregate in presence of salt even if they are stabilized by citrate [44]. This is the main issue for their detection by the nanopore technique, which consists of measuring an ionic current. To obtain stable nanoparticles, the latter were functionalized with SH-PEG. After functionalization, the AuNP were analysed by dynamic light scattering (DLS) to determine their hydrodynamic radius (Figure 3). From the autocorrelation functions, we obtained a range of nanoparticles of 38 nm, 64 nm, 71 nm, and 90 nm. The obtained diameters are larger than those of the starting nanoparticles. This increase is due to the aggregation of the particles, but also by the polymer layer. We selected this set of 4 AuNPs because no aggregation occurred after the addition of 1M NaCl as shown by both DLS measurements. In addition, no shift in the surface plasmon resonance (SPR) band was observed in absorbance measurements.

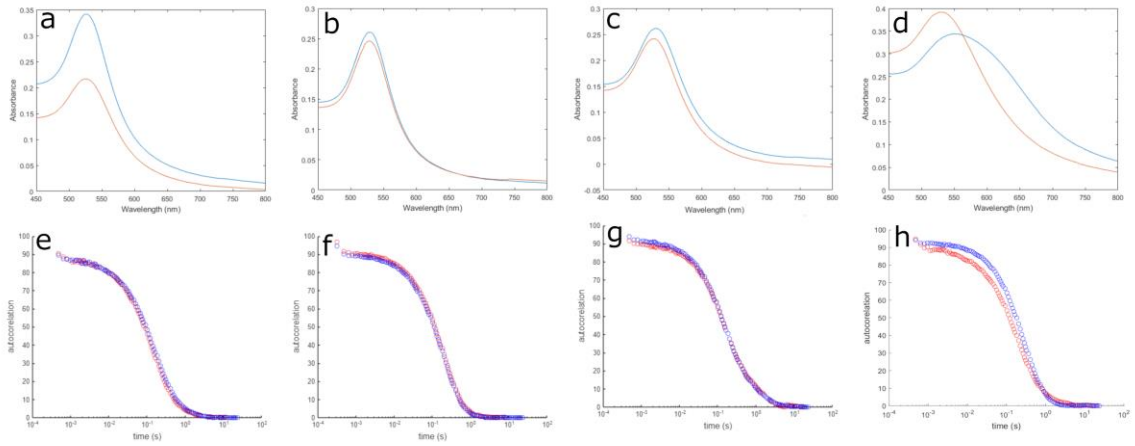

Figure 3: AuNP characterization and evaluation of the stability. The absorbance of AuNP functionalized with PEG diameter (a) 38 nm, (b) 64 nm, (c) 90 nm and (d) 71 nm under 1 M NaCl before (red) and after (blue) applying a voltage 3V across a multipore membrane for 1 H. Autocorrelation function of AuNP functionalized with PEG diameter (e) 38 nm, (f) 64 nm, (g) 90 nm and (h) 71 nm under 1 M NaCl before (red, circle) and after (blue, circle) applying a voltage 3V across a multipore membrane for 1 H.

The nanopore measurements were performed by applying a constant voltage between -1 V and -3.5 V. To evaluate the impact of the voltage and salt on their aggregation, the nanoparticles were placed in a half-cell containing a 1 M NaCl solution separated by a multipore membrane composed of a bullet-like shape nanopore (tip diameter 100 nm). A current of -2 V was applied for 10 minutes. DLS and absorbance measurements were performed at the beginning and end of the experiment. The results show no significant difference in the SPR band or the autocorrelation function for the nanoparticles of 38 nm, 64 nm, and 90 nm diameter. Thus, we can conclude that the PEG-coated NPs are stable under the conditions of the resistive pulse experiment. For the 71 nm nanoparticles, a shift in the SPR band and a shift in the autocorrelation function shows that the particles aggregate after 10 minutes. This may result in clogging of the nanopore if the detection experiment is too long.

3. Nanoparticles detection, impact of PEG chains

The detection of nanoparticles was achieved using two types of nanopores with tip diameters of 100 ± 30 nm and 130 ± 30 nm and the base around 330 nm. The AuNP-PEG was placed on the tip side and a voltage between -1 V and -3.5 V were applied on the opposite side. The passage of the AuNP-PEG induces a blockage of the ionic current, which is characterized by its relative amplitude ($\Delta I/I_{avg}$) and time (ΔT) (Figure 4).

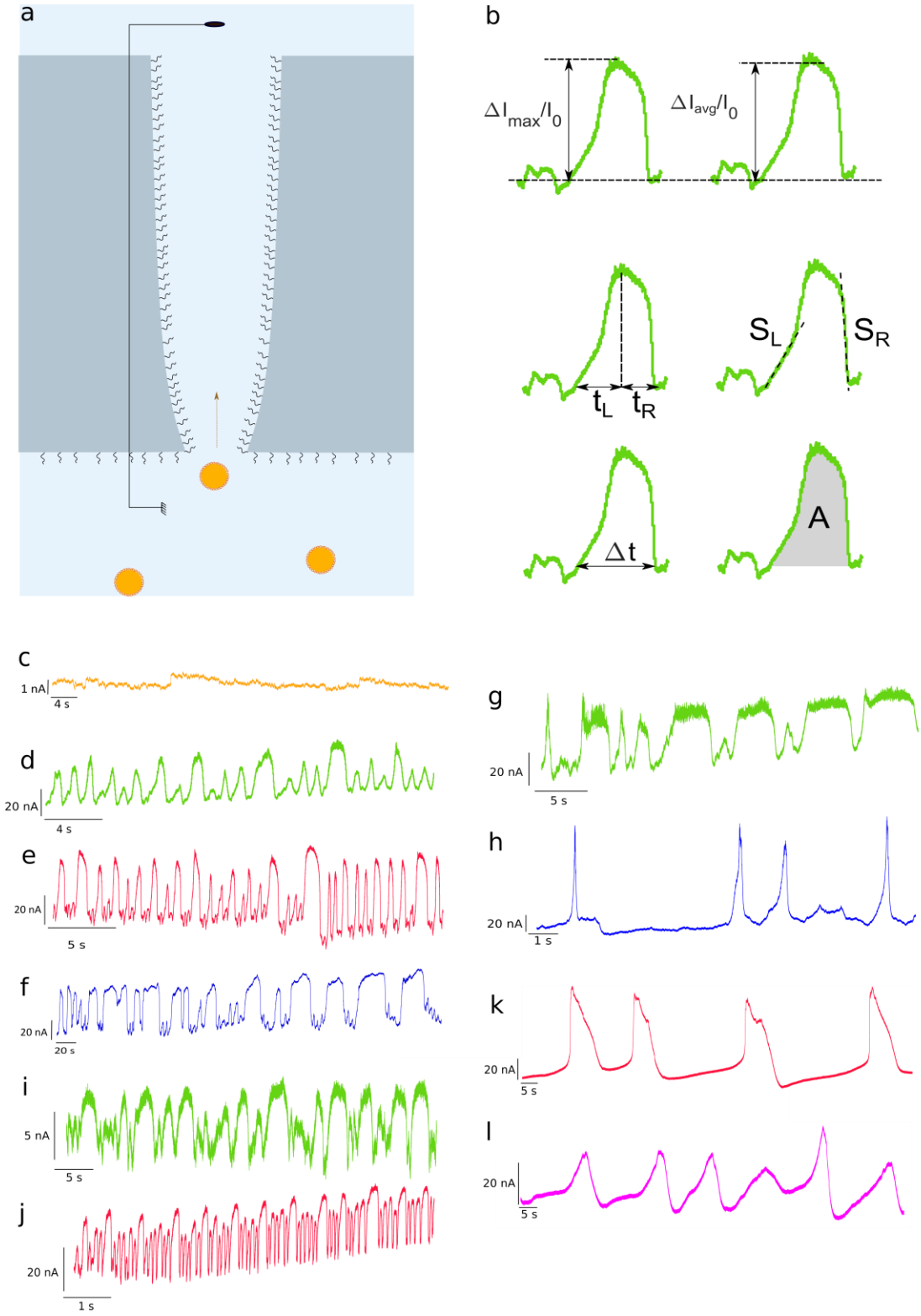

Figure 4: (a) Sketch of the AuNP-PEG detection using single bullet-like shape nanopore. (b) Zoom on an event and detail of the features used for the machine learning. (c) Examples of current trace obtained for the control. Examples of current

trace obtained for: Detection of (d) AuNP-PEG$_{38}$, (e) AuNP-PEG$_{64}$, (f) AuNP-PEG$_{71}$, using nanopore 100 nm diameter functionalized with PEG 20 kDa. Detection of (g) AuNP-PEG$_{38}$, (h) AuNP-PEG$_{71}$, using nanopore 100 nm diameter functionalized with PEG 5 kDa. Detection of (i) AuNP-PEG$_{38}$, (j) AuNP-PEG$_{64}$, using nanopore 130 nm diameter functionalized with PEG 20 kDa. Detection of (k) AuNP-PEG$_{64}$, (l) AuNP-PEG$_{90}$, using nanopore 130 nm diameter functionalized with PEG 5 kDa.

First, we investigate the impact of the nanopore diameter and the length of PEG chains on the AuNP-PEG detection. Indeed, we can hypothesize that the PEG will modify the nanopore diameter and its surface charge (due to the different grafted ratio) and thus have an influence on both the amplitude of the current blockage and the dwell time. To this end, the experiments were conducted with nanoparticles of diameters 64 and 71 nm using single nanopores of 100 nm and 130 nm tip diameter functionalized with either 5 kDa or 20 kDa PEGs. In Figure 5, distribution histograms of the current blockade amplitude are reported, as well as the scatter plot ΔI/I vs ΔT obtained AuNP-PEG$_{71}$ (concentrate to 1,495.10^{10} particles/ml) detected by a nanopore of diameter 100 ± 30 nm. For the nanopore functionalized by PEG 5 kDa, the distribution of ΔI/I is centred on a value of 0.192 whereas it shifts toward 0.223 for the nanopore functionalized with PEG 20 kDa chain. It is also interesting to note that the value of the dwell times is in the order of a second. This is explained by the crowding of the nanopore induced by the polymer chain as shown previously with the detection of amyloids [14]. A similar experiment with AuNP-PEG$_{64}$ (concentrate to 4,475.10^{9} particles/ml) using a larger nanopores (tip diameter 130 ± 30 nm) was performed. The results also show a shift in the distribution of the ΔI/I distribution with the length of PEG. Typically, the distributions are centred on 0.092 and 0.179 for the nanopores functionalized with PEG 5 kDa and 20 kDa PEG respectively. In addition, we observe that these ΔI/I values are lower than those obtained for NPs of similar sizes with a 100 nm diameter nanopore. This is in good agreement with the fact that the volume occupied by an AuNP-PEG$_{64}$ inside a nanopore with diameter 130 nm is lower than the one occupied by a AuNP-PEG$_{71}$ inside a nanopore with a diameter of around 100 nm. Interestingly, the dwell times are also dependent on the diameter of the nanopores. Indeed, for a 100 nm diameter nanopore the median dwell times are in the order of a second (2.3 and 1.7 for PEG lengths of 5 kDa and 20 kDa, whereas for a 130 nm diameter nanopore the residence times are 0.48 s and 0.32 s). This can be attributed to the difference of crowding where the AuNP-PEG is slowing down by the PEG chain when the nanopore is smaller. Unfortunately, it is difficult to determine the capture under equilibrium to evaluate the impact of nanopore properties on the entrance energy of the AuNP-PEG. However, we have demonstrated in this section that both the nanopore diameter and the PEG length have an impact on the signal of the AuNP-PEG detection.

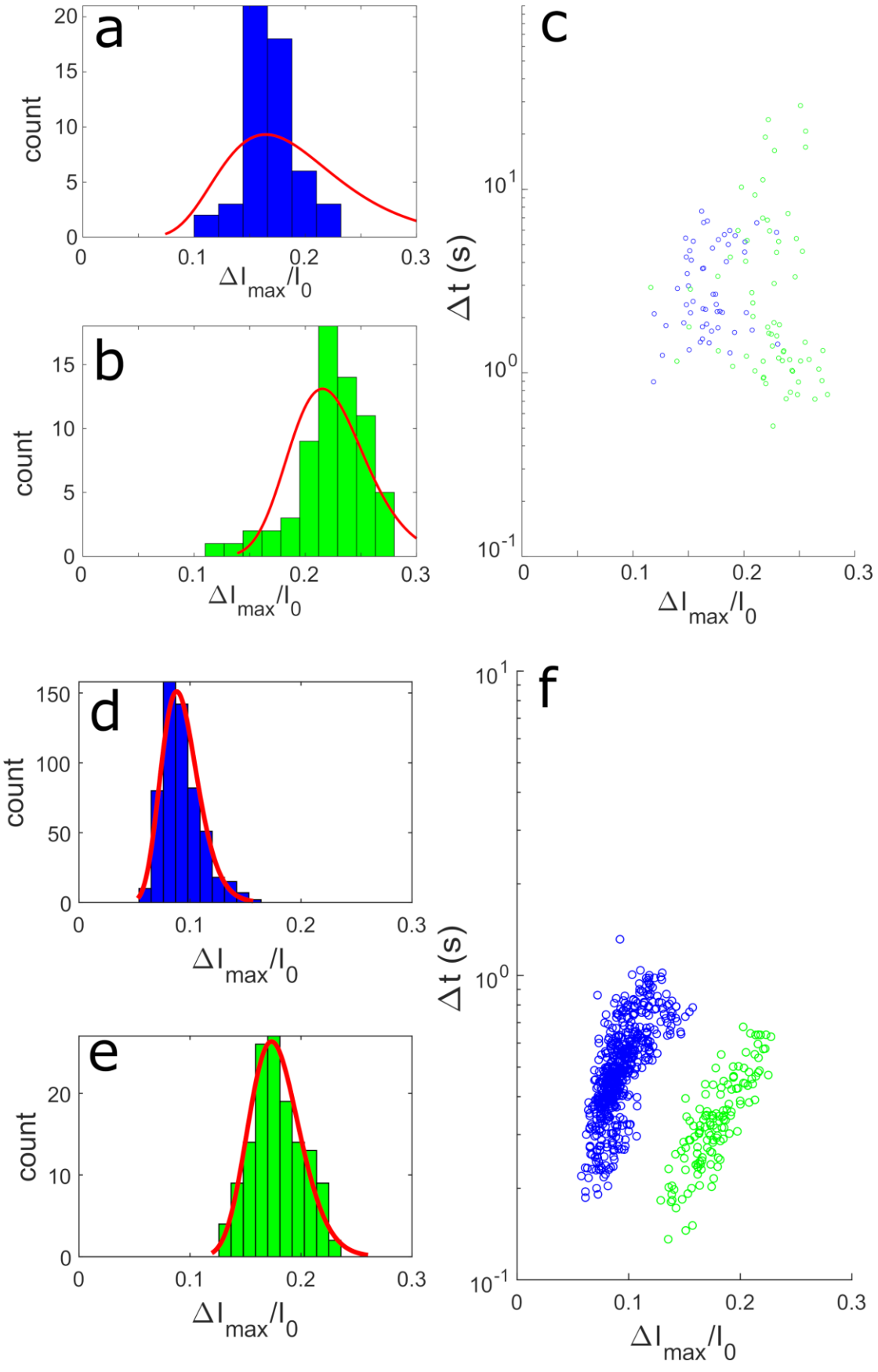
a
b
c
d
e
f
count
Δt (s)
ΔI_max/I_0

Figure 5: Impact of nanopore diameter and PEG Mw on the AuNP-PEG detection. AuNP-PEG$_{71}$ (concentrate to 1,495.10^{10} particles/ml) detection by nanopore diameter 100 nm ± 30 nm functionalized with PEG 5 k Da (blue) and 20 kDa (green) (a), (b) distribution histogram of ΔI/I and (c) scatter plot ΔI/I$_0$ vs Δt. AuNP-PEG$_{64}$ (concentrate to 4,475.10^9 particles/ml) detection by nanopore diameter 130 nm ± 30 nm functionalized with PEG 5 k Da (blue) and 20 kDa (green) (d), (e) distribution histogram of ΔI/I and (f) scatter plot ΔI/I$_0$ vs Δt.

4. Nanoparticle discrimination

The different functionalized nanopores were then used to discriminate between nanoparticles of different diameters. First, we considered the nanopores independently according to their diameter and the size of the PEGs chain used for the functionalization. Indeed, we have previously shown that each of these parameters has an impact on the amplitude of the ΔI/I vs Δt. The scatter plots representing the ΔI/I vs Δt are plotted in Figure 6 for nanopores of diameter 100 nm and 130 nm functionalized with PEGs of length 5 kDa and 20 kDa. The concentrations of nanoparticles were 1,635.10^{10} particles/ml for AuNP-PEG$_{38}$ and AuNP-PEG$_{90}$, 4,475.10^9 particles/ml for AuNP-PEG$_{64}$ and 1,495.10^{10} particles/ml for AuNP-PEG$_{71}$.

Initially, we focused on the amplitude of the blockage to try to discriminate the different nanoparticles analysed with the nanopores. This parameter is independent of the voltage applied for the same nanopore. Then, the dwell time was taken into account since it depends on the applied voltage, the charge of the nanoparticles, and their diffusion coefficient inside the nanopore.

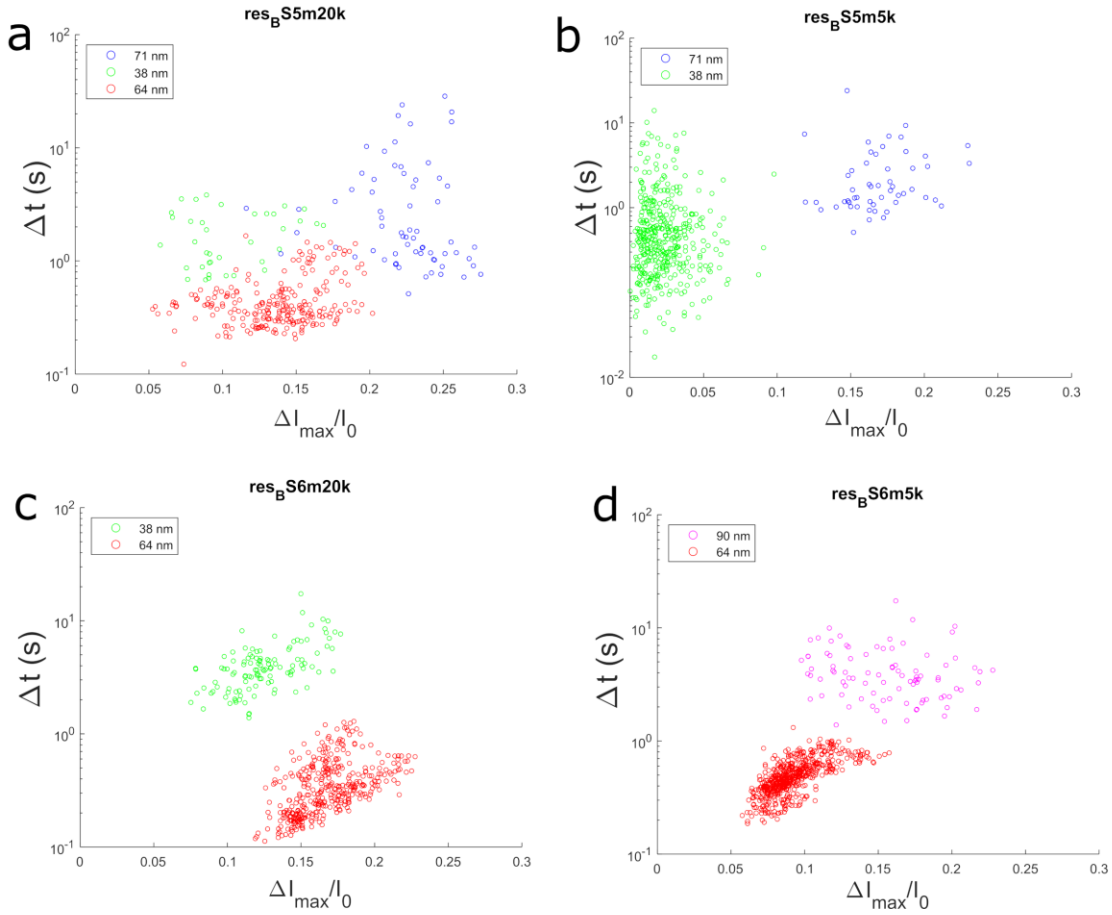

Figure 6: Scatter plot of ΔI/I vs Δt obtain by the detection of (a) AuNP-PEG$_{38}$ (green), AuNP-PEG$_{64}$ (red), AuNP-PEG$_{71}$ (blue), using nanopore 100 nm diameter functionalized with PEG 20 kDa, (b) AuNP-PEG$_{38}$ (green), AuNP-PEG$_{71}$ (bleu), using nanopore 100 nm diameter functionalized with PEG 5 kDa, (c) AuNP-PEG$_{38}$ (green), AuNP-PEG$_{64}$ (red), using nanopore 130 nm diameter functionalized with PEG 20 kDa, (d) AuNP-PEG$_{90}$ (magenta), AuNP-PEG$_{64}$ (red), using nanopore 130 nm diameter functionalized with PEG 5 kDa.

For the 100 nm diameter nanopore functionalized with 20 kDa PEGs, the ΔI/I distributions allow clear discrimination of nanoparticles of AuNP-PEG$_{38}$ and Au-PEG$_{71}$. They overlap the ΔI/I distributions of AuNP-PEG$_{64}$. Nevertheless, the centres of the distributions, 0.104, 0.137, and 0.224, for nanoparticle diameters of 38 nm, 64 nm, and 71 nm, respectively are significantly different. By functionalizing the nanopore with PEG 5 kDa, we also notice that the ΔI/I allow the discrimination of nanoparticles of diameters 38 nm and 71 nm. The detections of the nanoparticles carried out with a 130 nm diameter nanopore functionalized with a 20 kDa PEG chain show, as for the 100 nm nanopore, an overlap of the ΔI/I distributions of AuNP-PEG$_{38}$ and AuNP-PEG$_{64}$ even though the distribution centres of 0.125 and 0.1658 respectively are different. For the nanopore functionalized with a 5 kDa PEG chain, the 38 nm nanoparticles could not be detected. However, the ΔI/I distributions shifted to larger values (0.092 and 0.156 for 64 nm and 90 nm diameter nanoparticles respectively). Nevertheless, the distributions overlap, making it difficult to discriminate between samples

on this single parameter. Regardless of the nanopore, the discrimination of the different AuNP-PEG is better once the dwell time is considered. Indeed, the Δt of AuNP-PEG_{64} is shorter than the other. In this case, the cloud dots are perfectly separated making the discrimination of the AuNP-PEG suitable.

5. Machine learning

We have demonstrated the possibility to discriminate different nanoparticles using nanopores of similar diameter and functionalization. However, the problems that can be encountered with solid or polymeric nanopores is the inherent variability of their size. That does not exist in biological nanopores. Thus, it is essential to be able to discriminate between samples using nanopores with different diameters to expect to merge several experiments. To do this, a simple analysis of blockade amplitude and time is not sufficient. The current blockages can be characterized by several parameters as we have previously reported [40] (Figure 3). Thus, for each event we have reported the average ($\Delta I_{av}/I$) and maximum ($\Delta I_{max}/I$) relative amplitude. These two values differ since the maximum amplitude is assumed to be the one obtained when the nanoparticle is located exactly at the entrance of the nanopore whereas the average takes into account the passage of the entire asymmetric detection zone. In addition to the dwell time (Δt), we also noted the right (t_R) and left times (t_L) which are those relative to the time it takes for the nanoparticle to reach the entrance and to extract itself from the nanopore. These times make sense since the nanopore is asymmetric. We also defined the right (S_R) and left slopes (S_R) which are relative to the decrease and increase of the current as a function of time. The area (A) under the curve is a function of both the time and the amplitude of the blockage.

Thus, we defined for each blocking a set of 8 features to characterize each blockade event. To build the complete dataset using the different nanopores, it is important to include the diameter of the nanopore and the Mw of the PEG used for the functionalization. In addition, the parameters involving the time (*i.e.* Δt, t_R, t_L, S_R, S_L and A) are dependent on both the applied voltage and the properties of the nanoparticles. It is therefore essential to add the applied voltage as a feature in the dataset. The latter was built by the summation of all event parameters from the different nanopore. Then the datasets were split into two groups where 80% of the events were randomly selected to train the learning algorithm. The remaining 20% were used to test the algorithm. In order to discriminate the samples, we used a neural network classification learning. This supervised learning method is suitable for the present problem since it uses an interconnected data set. The input parameters are combined to define a hidden layer with the output, which in our case is the diameter of the nanoparticle.

The first set of analysis consists of training a neural network model with a dataset obtained from the detection of AuNP-PEG_{38} and AuNP-PEG_{64} using nanopore with diameters of 100 nm and 130 nm independently. The confusion matrices reported in Figure 7 shows for the 100 nm nanopore an error rate of less than 0.6% when training the algorithm. However, the accuracy of the test phase reaches 100%. For the 130 nm nanopores the result shows the accuracy of 100% in both the training and test phases. This

result is not surprising since the scatter plot shows a good discrimination of the nanoparticles. However, the contribution of the learner classification makes possible the nanoparticles discrimination even if the nanopore have different functionalization of applied voltage. Thus, it is possible to combine easily data coming from different nanopore experiment as soon as their characteristic becomes a feature implemented in the algorithm.

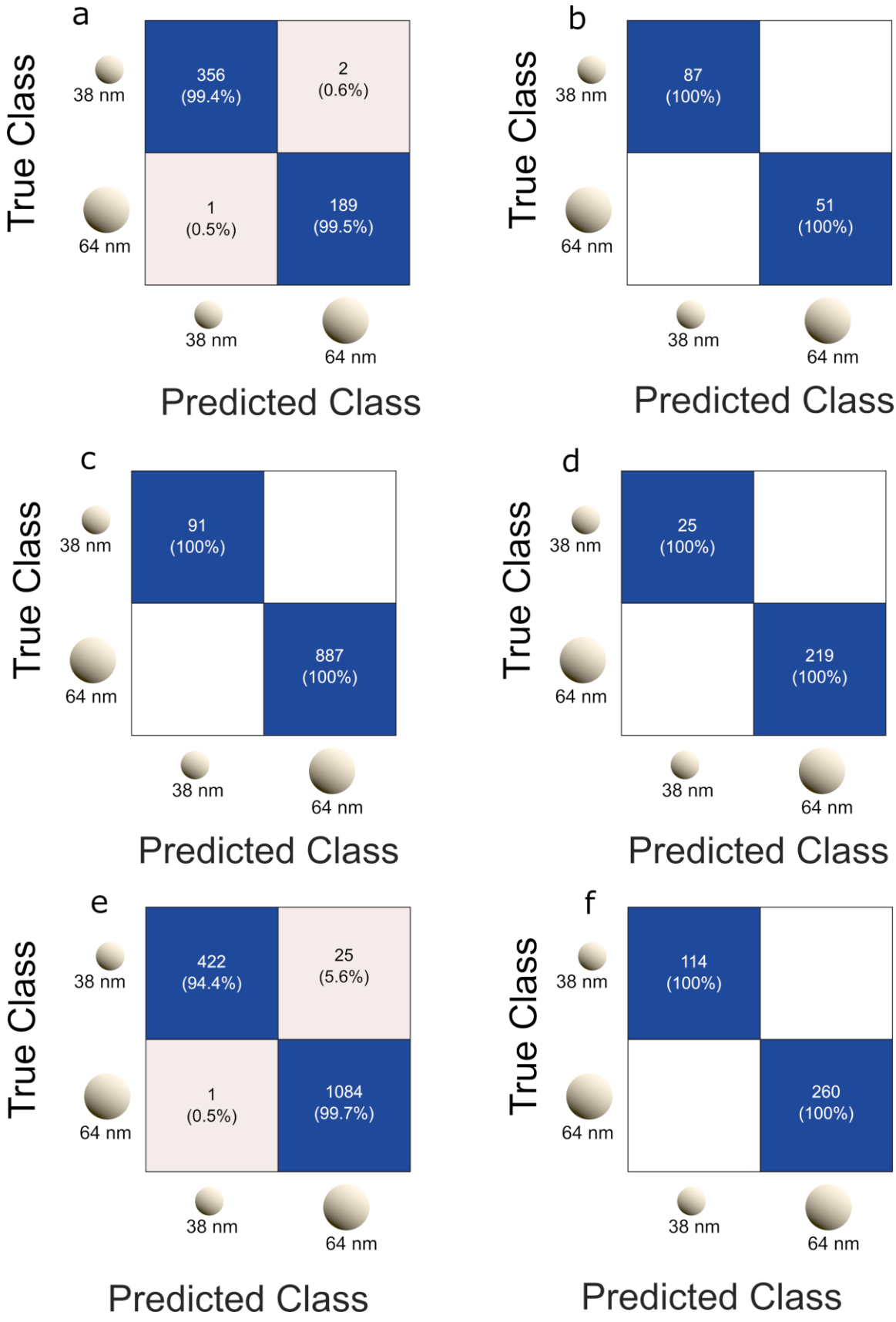
a
True Class
38 nm
64 nm
356
(99.4%)
2
(0.6%)
1
(0.5%)
189
(99.5%)
38 nm
64 nm
Predicted Class
b
True Class
38 nm
64 nm
87
(100%)
51
(100%)
38 nm
64 nm
Predicted Class
c
True Class
38 nm
64 nm
91
(100%)
887
(100%)
38 nm
64 nm
Predicted Class
d
True Class
38 nm
64 nm
25
(100%)
219
(100%)
38 nm
64 nm
Predicted Class
e
True Class
38 nm
64 nm
422
(94.4%)
25
(5.6%)
1
(0.5%)
1084
(99.7%)
38 nm
64 nm
Predicted Class
f
True Class
38 nm
64 nm
114
(100%)
260
(100%)
38 nm
64 nm
Predicted Class

Figure 7: Confusion matrices (a) training and (b) test showing the capability to discriminate the AuNP-PEG $_{38}$ and AuNP-PEG $_{64}$ using nanopore with diameter 100 nm. Confusion matrices (c) training and (d) tests showing the capability to discriminate the AuNP-PEG $_{38}$ and AuNP-PEG $_{64}$ using nanopore with diameter 130 nm. Confusion matrices (e) training and (f) tests showing the capability to discriminate the AuNP-PEG $_{38}$ and AuNP-PEG $_{64}$ using bullet shape nanopore with different nanopore size, functionalization and voltage.

To go further, we trained the neural network algorithm with data from nanopores with different diameters and functionalization. The interest here is to be able to accumulate independent experiments. The results represented on the confusion matrix show that in the training session the accuracy is 95.4% for Au-NP-PEG_{38} and 99.5% for AuNP-PEG_{64} nm nanoparticles. However, in the test phase the accuracy is 100%, *i.e.* the algorithm correctly classifies both types of nanoparticles. This shows that even if track etched nanopores are not *a priory* the most efficient choice for nanoparticle discrimination because of their unpredictable geometry, when combined with machine learning they can be an ally of choice for the development of precision analytical techniques.

Conclusion

To sum up, the present work was motivated in the overcoming of the limitation of the track-etched nanopore to cumulate different independent experiments in discriminating the same sample. To this end we have designed a bullet-like shape nanopore with diameter about 100 nm and 130 nm functionalized with PEG 5 kDa and 20 kDa. The detection of a set of AuNP-PEG shows an influence of both the nanopore diameter and PEG size. To discriminate the nanoparticle, the relative current blockade is not sufficient for the nanopore with diameter 130 nm. However, the use of two parameters ($\Delta I_{av}/I$, Δt) allows the sample discrimination using each nanopore independently. We define each event from the independent experiment with set of 8 and 3 features to define the blockade and the nanopore respectively. The use of neuronal network classification shows the accuracy of 100% for the testing when all the independent experiments are cumulated. This result proves that despite the variability of the track-etched nanopore size and surface state, the use of machine learning allows discriminating samples from several independent experiments as for the biological nanopore. Knowing that the variability of nanopore size after fabrication also exist for the SiN drill by controlled dielectric breakdown and the nanopore pulling, such approach could be easily extended to all solid-state nanopores.

Acknowledgements

This work was founded by Agence Nationale de la Recherche (ANR-19-CE42-0006, NanoOligo) and l'institut Carnot Chimie Balard Cirimat (ref16CARN000801). Single tracks have been produced in GANIL (Caen, France) in the framework of an EMIR project. The authors thank E. Balanzat and Y. NGono-Ravache at CIMAP Caen for support to produce tracked polymer film.

References

[1] L. Xue, H. Yamazaki, R. Ren, M. Wanunu, A.P. Ivanov, J.B. Edel, Solid-state nanopore sensors, Nat Rev Mater 5 (2020) 931–951. https://doi.org/10.1038/s41578-020-0229-6.

[2] Y. Wu, J.J. Gooding, The application of single molecule nanopore sensing for quantitative analysis, Chemical Society reviews 51 (2022) 3862–3885. https://doi.org/10.1039/d1cs00988e.

[3] Y. He, M. Tsutsui, Y. Zhou, X.-S. Miao, Solid-state nanopore systems: from materials to applications, NPG Asia Mater 13 (2021). https://doi.org/10.1038/s41427-021-00313-z.

[4] M. Drndić, 20 years of solid-state nanopores, Nat Rev Phys 3 (2021) 606. https://doi.org/10.1038/s42254-021-00363-w.

[5] H. Bayley, C.R. Martin, Resistive-Pulse Sensing-From Microbes to Molecules, Chemical reviews 100 (2000) 2575–2594. https://doi.org/10.1021/cr980099g.

[6] J.J. Kasianowicz, E. Brandin, D. Branton, D.W. Deamer, Characterization of individual polynucleotide molecules using a membrane channel, Proceedings of the National Academy of Sciences of the United States of America 93 (1996) 13770–13773. https://doi.org/10.1073/pnas.93.24.13770.

[7] R.W. DeBlois, C.P. Bean, Counting and Sizing of Submicron Particles by the Resistive Pulse Technique, Review of Scientific Instruments 41 (1970) 909–916. https://doi.org/10.1063/1.1684724.

[8] R.W. DeBlois, E.E. Uzgiris, D.H. Cluxton, H.M. Mazzone, Comparative measurements of size and polydispersity of several insect viruses, Analytical Biochemistry 90 (1978) 273–288. https://doi.org/10.1016/0003-2697(78)90032-5.

[9] E. Weatherall, P. Hauer, R. Vogel, G.R. Willmott, Pulse Size Distributions in Tunable Resistive Pulse Sensing, Analytical chemistry 88 (2016) 8648–8656. https://doi.org/10.1021/acs.analchem.6b01818.

[10] Z. Qin, J. Zhe, G.-X. Wang, Effects of particle's off-axis position, shape, orientation and entry position on resistance changes of micro Coulter counting devices, Meas. Sci. Technol. 22 (2011) 45804. https://doi.org/10.1088/0957-0233/22/4/045804.

[11] C. Ying, J. Houghtaling, M. Mayer, Effects of off-axis translocation through nanopores on the determination of shape and volume estimates for individual particles, Nanotechnology 33 (2022). https://doi.org/10.1088/1361-6528/ac6087.

[12] E.C. Yusko, B.R. Bruhn, O.M. Eggenberger, J. Houghtaling, R.C. Rollings, N.C. Walsh, S. Nandivada, M. Pindrus, A.R. Hall, D. Sept, J. Li, D.S. Kalonia, M. Mayer, Real-time shape approximation and fingerprinting of single proteins using a nanopore, Nature nanotechnology 12 (2017) 360–367. https://doi.org/10.1038/nnano.2016.267.

[13] L. Bacri, A.G. Oukhaled, B. Schiedt, G. Patriarche, E. Bourhis, J. Gierak, J. Pelta, L. Auvray, Dynamics of colloids in single solid-state nanopores, The journal of physical chemistry. B 115 (2011) 2890–2898. https://doi.org/10.1021/jp200326w.

[14] N. Meyer, N. Arroyo, J.-M. Janot, M. Lepoitevin, A. Stevenson, I.A. Nemeir, V. Perrier, D. Bougard, M. Belondrade, D. Cot, J. Bentin, F. Picaud, J. Torrent, S. Balme, Detection of Amyloid-β Fibrils Using Track-Etched Nanopores: Effect of Geometry and Crowding, ACS sensors 6 (2021) 3733–3743. https://doi.org/10.1021/acssensors.1c01523.

[15] N. Meyer, J.-M. Janot, J. Torrent, S. Balme, Real-Time Fast Amyloid Seeding and Translocation of α-Synuclein with a Nanopipette, ACS central science 8 (2022) 441–448. https://doi.org/10.1021/acscentsci.1c01404.

[16] B. Huang, L. Miao, J. Li, Z. Xie, Y. Wang, J. Chai, Y. Zhai, Identification of plasmon-driven nanoparticle-coalescence-dominated growth of gold nanoplates through nanopore sensing, Nature communications 13 (2022) 1402. https://doi.org/10.1038/s41467-022-29123-9.

[17] S. Balme, M. Lepoitevin, L.F. Dumée, M. Bechelany, J.-M. Janot, Diffusion dynamics of latex nanoparticles coated with ssDNA across a single nanopore, Soft Matter 13 (2017) 496–502. https://doi.org/10.1039/C6SM02461K.

[18] G. Goyal, K.J. Freedman, M.J. Kim, Gold nanoparticle translocation dynamics and electrical detection of single particle diffusion using solid-state nanopores, Analytical chemistry 85 (2013) 8180–8187. https://doi.org/10.1021/ac4012045.

[19] W.-J. Lan, D.A. Holden, B. Zhang, H.S. White, Nanoparticle transport in conical-shaped nanopores, Analytical chemistry 83 (2011) 3840–3847. https://doi.org/10.1021/ac200312n.

[20] J. Kong, H. Wu, L. Liu, X. Xie, L. Wu, X. Ye, Q. Liu, Silicon nitride nanopores for nanoparticle s ensing, Journal of nanoscience and nanotechnology 13 (2013) 4010–4016. https://doi.org/10.1166/jnn.2013.7141.

[21] M. Tsutsui, T. Yamazaki, K. Tatematsu, K. Yokota, Y. Esaki, Y. Kubo, H. Deguchi, A. Arima, S.'i. Kuroda, T. Kawai, High-throughput single nanoparticle detection using a feed-through channel-integrated nanopore, Nanoscale 11 (2019) 20475–20484. https://doi.org/10.1039/C9NR07039G.

[22] A. Arima, M. Tsutsui, T. Washio, Y. Baba, T. Kawai, Solid-State Nanopore Platform Integrated with Machine Learning for Digital Diagnosis of Virus Infection, Analytical chemistry 93 (2021) 215–227. https://doi.org/10.1021/acs.analchem.0c04353.

[23] M. Taniguchi, S. Minami, C. Ono, R. Hamajima, A. Morimura, S. Hamaguchi, Y. Akeda, Y. Kanai, T. Kobayashi, W. Kamitani, Y. Terada, K. Suzuki, N. Hatori, Y. Yamagishi, N. Washizu, H. Takei, O. Sakamoto, N. Naono, K. Tatematsu, T. Washio, Y. Matsuura, K. Tomono, Combining machine learning and nanopore construction creates an artificial intelligence nanopore for coronavirus detection, Nature communications 12 (2021) 3726. https://doi.org/10.1038/s41467-021-24001-2.

[24] P. Apel, Track etching technique in membrane technology, Radiation Measurements 34 (2001) 559–566. https://doi.org/10.1016/S1350-4487(01)00228-1.

[25] T. Ma, J.-M. Janot, S. Balme, Track-Etched Nanopore/Membrane: From Fundamental to Applications, Small Methods 4 (2020) 2000366. https://doi.org/10.1002/smtd.202000366.

[26] T. Ma, N. Arroyo, J. Marc Janot, F. Picaud, S. Balme, Conformation of Polyethylene Glycol inside Confined Space: Simulation and Experimental Approaches, Nanomaterials (Basel, Switzerland) 11 (2021). https://doi.org/10.3390/nano11010244.

[27] S. Balme, F. Picaud, M. Manghi, J. Palmeri, M. Bechelany, S. Cabello-Aguilar, A. Abou-Chaaya, P. Miele, E. Balanzat, J.M. Janot, Ionic transport through sub-10 nm diameter hydrophobic high-aspect ratio nanopores: experiment, theory and simulation, Scientific reports 5 (2015) 10135. https://doi.org/10.1038/srep10135.

[28] P.Y. Apel, Y.E. Korchev, Z. Siwy, R. Spohr, M. Yoshida, Diode-like single-ion track membrane prepared by electro-stopping, Nuclear Instruments and Methods in Physics Research Section B: Beam Interactions with Materials and Atoms 184 (2001) 337–346. https://doi.org/10.1016/S0168-583X(01)00722-4.

[29] P.Y. Apel, I.V. Blonskaya, S.N. Dmitriev, O.L. Orelovich, B.A. Sartowska, Ion track symmetric and asymmetric nanopores in polyethylene terephthalate foils for versatile applications, Nuclear Instruments and Methods in Physics Research Section B: Beam Interactions with Materials and Atoms 365 (2015) 409–413. https://doi.org/10.1016/j.nimb.2015.07.016.

[30] Z.S. Siwy, Ion-Current Rectification in Nanopores and Nanotubes with Broken Symmetry, Adv. Funct. Mater. 16 (2006) 735–746. https://doi.org/10.1002/adfm.200500471.

[31] J. Cervera, B. Schiedt, R. Neumann, S. Mafé, P. Ramírez, Ionic conduction, rectification, and selectivity in single conical nanopores, The Journal of Chemical Physics 124 (2006) 104706. https://doi.org/10.1063/1.2179797.

[32] C.-Y. Lin, T. Ma, Z.S. Siwy, S. Balme, J.-P. Hsu, Tunable Current Rectification and Selectivity Demonstrated in Nanofluidic Diodes through Kinetic Functionalization, The journal of physical chemistry letters 11 (2020) 60–66. https://doi.org/10.1021/acs.jpclett.9b03344.

[33] M. Lepoitevin, T. Ma, M. Bechelany, J.-M. Janot, S. Balme, Functionalization of single solid state nanopores to mimic biological ion channels: A review, Advances in colloid and interface science 250 (2017) 195–213. https://doi.org/10.1016/j.cis.2017.09.001.

[34] T. Ma, E. Balanzat, J.-M. Janot, S. Balme, Single conical track-etched nanopore for a free-label detection of OSCS contaminants in heparin, Biosensors & bioelectronics 137 (2019) 207–212. https://doi.org/10.1016/j.bios.2019.05.005.

[35] N. Giamblanco, D. Coglitore, A. Gubbiotti, T. Ma, E. Balanzat, J.-M. Janot, M. Chinappi, S. Balme, Amyloid Growth, Inhibition, and Real-Time Enzymatic Degradation Revealed with Single Conical

Nanopore, Analytical chemistry 90 (2018) 12900–12908. https://doi.org/10.1021/acs.analchem.8b03523.

[36] N. Giamblanco, Y. Fichou, J.-M. Janot, E. Balanzat, S. Han, S. Balme, Mechanisms of Heparin-Induced Tau Aggregation Revealed by a Single Nanopore, ACS sensors 5 (2020) 1158–1167. https://doi.org/10.1021/acssensors.0c00193.

[37] N. Giamblanco, J.-M. Janot, A. Gubbiotti, M. Chinappi, S. Balme, Characterization of Food Amyloid Protein Digestion by Conical Nanopore, Small Methods 4 (2020) 1900703. https://doi.org/10.1002/smtd.201900703.

[38] M. Pevarnik, K. Healy, M.E. Toimil-Molares, A. Morrison, S.E. Létant, Z.S. Siwy, Polystyrene particles reveal pore substructure as they translocate, ACS nano 6 (2012) 7295–7302. https://doi.org/10.1021/nn302413u.

[39] Y. Qiu, C. Yang, P. Hinkle, I.V. Vlassiouk, Z.S. Siwy, Anomalous mobility of highly charged particles in pores, Analytical chemistry 87 (2015) 8517–8523. https://doi.org/10.1021/acs.analchem.5b02060.

[40] N. Meyer, J.-M. Janot, M. Lepoitevin, M. Smietana, J.-J. Vasseur, J. Torrent, S. Balme, Machine Learning to Improve the Sensing of Biomolecules by Conical Track-Etched Nanopore, Biosensors 10 (2020). https://doi.org/10.3390/bios10100140.

[41] L. Reynaud, A. Bouchet-Spinelli, J.-M. Janot, A. Buhot, S. Balme, C. Raillon, Discrimination of α-Thrombin and γ-Thrombin Using Aptamer-Functionalized Nanopore Sensing, Analytical chemistry 93 (2021) 7889–7897. https://doi.org/10.1021/acs.analchem.1c00461.

[42] M. Taniguchi, H. Takei, K. Tomiyasu, O. Sakamoto, N. Naono, Sensing the Performance of Artificially Intelligent Nanopores Developed by Integrating Solid-State Nanopores with Machine Learning Methods, J. Phys. Chem. C 126 (2022) 12197–12209. https://doi.org/10.1021/acs.jpcc.2c02674.

[43] P.Y. Apel, I.V. Blonskaya, S.N. Dmitriev, O.L. Orelovitch, A. Presz, B.A. Sartowska, Fabrication of nanopores in polymer foils with surfactant-controlled longitudinal profiles, Nanotechnology 18 (2007) 305302. https://doi.org/10.1088/0957-4484/18/30/305302.

[44] M. Lepoitevin, M. Lemouel, M. Bechelany, J.-M. Janot, S. Balme, Gold nanoparticles for the bare-eye based and spectrophotometric detection of proteins, polynucleotides and DNA, Microchim Acta 182 (2015) 1223–1229. https://doi.org/10.1007/s00604-014-1408-1.